



Kinetic Monte Carlo simulation on influence of vacancy on hydrogen diffusivity in tungsten



Takuji Oda ^{a,*}, Deqiong Zhu ^a, Yoshiyuki Watanabe ^b

^a Department of Nuclear Engineering, Seoul National University, 1 Gwanak-ro, Gwanak-gu, Seoul 151-742, South Korea

^b Japan Atomic Energy Agency, 2-166 Omotedate, Obuchi, Rokkasho, Kamikita, Aomori 039-3212, Japan

HIGHLIGHTS

- KMC simulation was performed to quantify the influence of vacancy-type trap in hydrogen diffusivity in tungsten.
- The simulation results indicated non-negligible influence of traps even at high temperatures like 1300 K.
- $D = 1.58 \times 10^{-7} \exp\left(-0.25 \frac{eV}{kT}\right) \text{m}^2 \text{s}^{-1}$, derived from experimental data above 1500 K, is recommended as H diffusivity in W.

ARTICLE INFO

Article history:

Received 3 March 2015

Received in revised form

30 July 2015

Accepted 31 July 2015

Available online 6 August 2015

Keywords:

Hydrogen diffusivity

Tungsten

Kinetic Monte Carlo simulation

Vacancy

ABSTRACT

Kinetic Monte Carlo (KMC) simulations are performed to quantify the influence of trap in hydrogen diffusivity in tungsten. As a typical trap, mono-vacancy is considered in the simulation. Experimental results reported by Frauenfelder are nicely reproduced when hydrogen concentration and trap concentration expected in the experiment are employed in the simulation. The effective diffusivity of hydrogen is evidently decreased by traps even at high temperatures like 1300 K. These results suggest that only high-temperature experimental data, which are not significantly affected by traps, should be fitted to, in order to derive the true hydrogen diffusivity from experiments. Therefore, we recommend $D = 1.58 \times 10^{-7} \exp(-0.25 \text{ eV}/kT) \text{ m}^2 \text{ s}^{-1}$ as the equation for hydrogen diffusion coefficient in tungsten, which was obtained by fitting only to experimental data at 1500–2400 K by Heinola and Ahlgren, rather than the most cited equation $D = 4.1 \times 10^{-7} \exp(-0.39 \text{ eV}/kT) \text{ m}^2 \text{ s}^{-1}$, which was obtained by fitting to all experimental data at 1100–2400 K including some data that should be affected by traps.

© 2015 Elsevier B.V. All rights reserved.

1. Introduction

In fusion reactors, since tritium balance between production in breeding materials and consumption in plasma will be tight [1,2], tritium retention in reactor materials needs to be minimized for establishing an efficient and sustainable tritium fuel cycle. Large tritium retention also causes radiation-safety concerns as tritium is radioactive. Therefore, understanding and controlling tritium behavior such as release and accumulation in reactor materials is an important subject in fusion engineering.

Among various materials to be used in fusion reactors, materials of plasma-facing components (PFCs) directly face to plasma and thus a large amount of tritium may be piled up in it. As a candidate

material for PFCs, tungsten and tungsten-based alloys have received increasing attention due to its high melting point, low erosion rate, and low hydrogen solubility (1.0 eV as the solution energy by first-principles calculation [3] and 1.16 eV as the activation energy for solution by experiment [4,5]). However, it has been shown that hydrogen retention is largely increased by irradiation defects [6–8]. For example, a mono-vacancy can trap multiple hydrogen atoms [9,10]. Therefore, many researches have been performed for understanding the influence of radiation defects on tritium behavior in tungsten [11–13].

The diffusion coefficient of hydrogen is one of the fundamental physical quantities that govern the tritium behavior in tungsten. It is directly relevant with tritium release and permeation from/through tungsten. In addition, it is a vital input in analyzing experimental results of thermal desorption spectroscopy (TDS; or temperature programmed desorption, TPD), which has been widely conducted to acquire information on hydrogen-defect interactions.

* Corresponding author.

E-mail address: oda@snu.ac.kr (T. Oda).

Among several reported hydrogen diffusivities, the equation given by Frauenfelder [14] has been most utilized:

$$D = 4.1 \times 10^{-7} \exp(-0.39 \text{ eV}/kT), \quad (1)$$

where D ($\text{m}^2 \text{ s}^{-1}$) is the diffusion coefficient of hydrogen at temperature T (K), and k ($=8.62 \times 10^{-5} \text{ eV K}^{-1}$) is the Boltzmann constant. This formula was determined by degassing experiment of pre-loaded H_2 gas in 1100–2400 K [14].

First-principles calculation based on density functional theory (DFT) has also been applied to hydrogen in tungsten. For achieving a diffusion coefficient, DFT calculation is often coupled with transition state theory (TST). For example in bcc-Fe, DFT + TST approach produced diffusion coefficients comparable with experimental results [15,16]. Since bcc-Fe has similar characteristics to bcc-W in respect to hydrogen behavior, such as a positive solution energy and a low energy barrier for hydrogen diffusion, it is reasonable to expect a good result in tungsten as well. However, previous DFT calculations showed large disagreement with experiment in the case of tungsten: 0.20 eV as the migration barrier in DFT calculation [17] and 0.39 eV as the activation energy for diffusion in Frauenfelder's experiment [14] (Eq. (1)). Note that the migration barrier reported by Johnson and Carter [18], 0.42 eV and 0.39 eV with zero-point energy correction, was calculated along a higher-barrier path via octahedral site (O-site), not along the minimum-barrier path via trigonal site (Tri-site). Therefore, it is inappropriate to compare this calculation value with the experimental value.

Heinola and Ahlgren [19] examined the disagreement between DFT calculation and Frauenfelder's experiment by using DFT + TST approach. They showed that the diffusion coefficients obtained with DFT + TST approach are comparable with those of Frauenfelder's experiment, if experimental data at low temperatures (<1500 K) are excluded. The exclusion decreases the activation energy for hydrogen diffusion in Frauenfelder's experiment from 0.39 eV to 0.25 eV, as given in the following Arrhenius equation [19]:

$$D = 1.58 \times 10^{-7} \exp(-0.25 \text{ eV}/kT). \quad (2)$$

This finding indicates significant influence of lattice defects which act as hydrogen traps up to high temperatures like 1500 K. Indeed, the influence of defects has been considered to be a main cause of scattering of hydrogen diffusion coefficients [20]. However, the influence is yet to be clearly quantified.

In the present study, we quantify the influence of traps in hydrogen diffusivity in bcc-W, in order to verify the Heinola's suggestion and Eq. (2). For this aim, we perform Kinetic Monte Carlo (KMC) simulation utilizing diffusion coefficients given by Eq. (2). Among several lattice defects which can act as hydrogen traps including grain boundary [21] and dislocation [22], we focus on vacancy in this study as a typical trap. Vacancy-hydrogen (V–H) interactions are modeled based on DFT calculation results reported by Ohsawa et al. [10]. Diffusion coefficients determined by KMC simulations in systems with and without vacancies are compared with those of Frauenfelder's experiment.

2. Computational method

2.1. Kinetic models in KMC

KMC simulation pursues a system evolution by repeating some atomic-scale kinetic events that are relevant with a phenomenon of interest. Judgment whether an event attempt will succeed or fail is made using Monte Carlo simulation technique. For example, when the success probability of an event per attempt is p ($0 < p < 1$), this

event will occur if a fraction, which is randomly generated between 0 and 1, is smaller than p . The frequency of event attempt is determined so that the expected frequency of event to succeed becomes consistent with the reaction rate in a kinetic model employed in the KMC simulation. The event frequency ν_{event} (s^{-1}) is given as follows:

$$\nu_{event} = \nu_{attempt} \times p = \nu_{attempt} \times \exp(-E/kT) \quad (3)$$

where $\nu_{attempt}$ (s^{-1}) is the attempt frequency of the event, p is the success probability of the event per attempt, and E (eV) is the activation energy for the event.

In the present KMC simulation, the phenomenon of interest is hydrogen diffusion in bcc-W where vacancies exist as traps. For this phenomenon, we consider three kinetic events: (i) migration of H atom in bcc lattice, (ii) trap of H atom by a vacancy, and (iii) detrap of H atom from a vacancy. Details of the three kinetic events are described below. Possible errors in this simple model are discussed in Chapter 4.

2.1.1. Migration event

In general, the diffusion coefficient of impurity atom such as H atom is expressed as

$$D = \frac{1}{6} f d^2 \Gamma, \quad (4)$$

where D ($\text{m}^2 \text{ s}^{-1}$) is the diffusion coefficient, $1/6$ is a factor for 3-dimensional diffusion, f (unitless) is the correlation factor, d (m) is the migration length of H atom per jump, and Γ (s^{-1}) is the jump frequency of H atom.

The correlation factor depends on diffusion mechanism. It is equal to 1, if atomic jumps isotropically and randomly occur, and thus if there is no correlation in sequential jumps. When hydrogen concentration is not extremely high, $f = 1$ is quite reasonable for hydrogen diffusion in bcc-W, because there is no significant binding interaction between two solute H atoms [17].

In bcc metals in general, including tungsten, tetrahedral site (T-site) is a stable site for H atom. Fig. 1 depicts some T-sites and migration paths. The lattice is shifted from a conventional one so that a T-site at which we assume that a H atom originally exists is located at the center. This T-site is colored red and labeled #1 in Fig. 1. For each T-site, there are four first neighboring T-sites and 2 s-neighboring T-sites. In Fig. 1, for #1 T-site, the first neighboring T-sites are labelled #2–#5 (blue), and the second-neighboring T-sites are labelled #6–#7 (green), respectively. Four paths to the first-

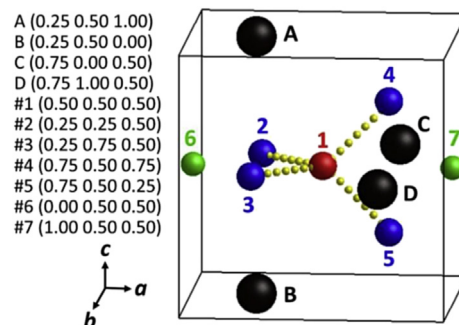


Fig. 1. Locations and migration paths of H atom in W crystal. Black spheres represent W atoms. Red, blue and green spheres represent T-sites where H atom can be located. Yellow spheres indicate available migration paths of H atom when located at #1 T-site. (For interpretation of the references to colour in this figure legend, the reader is referred to the web version of this article.)

neighboring T-sites are the minimum-barrier paths, which are displayed by yellow spheres in Fig. 1. The transition state along this minimum-barrier path is Tri-site, which is located at the middle of the path. Hence, $d = a_0/2\sqrt{2}$ is obtained as the distance between closest neighboring T-sites, where a_0 is the lattice constant of bcc-W. Since the thermal expansion of bcc-W is small, e.g. $\sim 0.4\%$ in linear expansion at 1000 K [23], a_0 can be regarded as a constant (3.16 Å as an extrapolation at 0 K [24]). Consequently, $1/6fd^2$ in Eq. (4) is equal to $2.08 \times 10^{-21} \text{ m}^2$, which is independent of the sort of hydrogen isotopes.

Γ can be further written down as follows:

$$\Gamma = n \times \nu \times \exp(-E/kT) \quad (5)$$

where n is the number of effective migration paths for each H atom, ν (s^{-1}) is the attempt frequency of jump to a neighboring site for each migration path, and E (eV) is the activation energy for migration. In bcc lattice, because each T-site has four first-neighboring T-sites as shown in Fig. 1, n is set to be 4. Consequently, ν is determined to be $1.90 \times 10^{13} \text{ s}^{-1}$ with $E = 0.25 \text{ eV}$ so that Eq. (2) is reproduced. Note that the attempt frequency and the activation energy used in the present kinetic model are fairly consistent with those determined by DFT calculation: 0.20 eV and $2.6 \times 10^{13} \text{ s}^{-1}$ (26 THz) [19], respectively.

2.1.2. Trap event

Fig. 2 depicts three key sites for trap and detrap events around a vacancy: first-neighboring T-site to the vacancy (1st-V-neig-T-site), second-neighboring T-site to the vacancy (2nd-V-neig-T-site) and first neighboring O-site to the vacancy (1st-V-neig-O-site).

In the present KMC model, a trap event corresponds to a migration event from a 2nd-V-neig-T-site to a 1st-V-neig-T-site. If this occurs, the state of hydrogen is changed from “solute” state to “trapped” state. DFT calculation showed that when H atoms are trapped by a vacancy, H atoms are located at around 1st-V-neig-O-sites or 1st-V-neig-T-sites [10]. The former is energetically favorable when the number of trapped H atoms in a vacancy is one or two, while the latter is so when more H atoms are trapped [10].

The present KMC model assumes that trapped H atoms are randomly located over twenty-four 1st-V-neig-T-sites, and that a

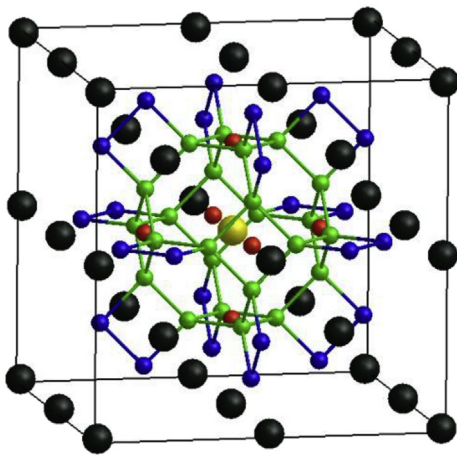


Fig. 2. Key sites for trap and detrap events around a vacancy. Black and yellow spheres represent W atoms and a W vacancy, respectively. Red spheres represent first-neighboring O-sites to the vacancy. Green and blue spheres represent first and second neighboring T-sites to the vacancy, respectively. Connections between some of them indicate migration paths of H atom. (For interpretation of the references to colour in this figure legend, the reader is referred to the web version of this article.)

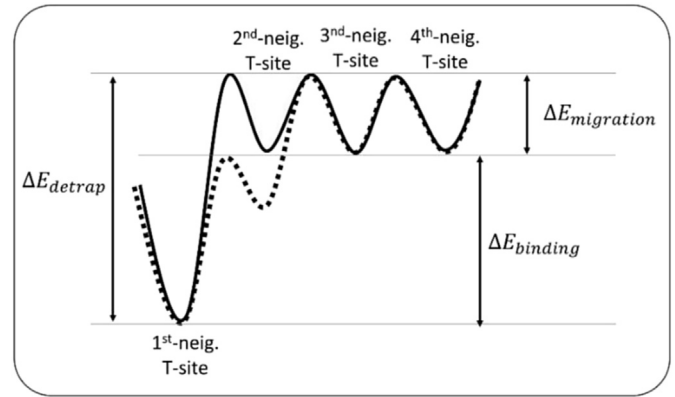


Fig. 3. Potential energy curve near a vacancy. The solid line schematically draws the one assumed in the present KMC model, while the dashed line the one expected from DFT calculation result [9].

trapped H atom jumps into a 2nd-V-neig-T-site, which is again randomly selected, if a detrap event occurs. These assumptions are reasonable because the barriers for migration between a 1st-V-neig-O-site and a 1st-V-neig-T-site and between 1st-V-neig-T-sites should be much smaller than energy barriers for detrap events, and thus a trapped H atom frequently changes its position before detraping.

The maximum number of H atoms that can be trapped by a vacancy is set to be twelve according to a result of DFT calculation [10]. Thus, twelve 1st-V-neig-T-sites (out of twenty-four) for each vacancy can be occupied by H atoms at most.

For trap event, the same attempt frequency and the same activation energy with those for migration event are set: $\nu_{\text{attempt}} = 1.90 \times 10^{13} \text{ s}^{-1}$ and $E = 0.25 \text{ eV}$. This means that the potential energy surface for H atom is assumed to be deformed just in the vicinity of vacancy, as schematically drawn in Fig. 3, although the deformation is induced over a somewhat longer range [9] in reality.

2.1.3. Detrap event

For detrap event of H atom from a vacancy, we use the same attempt frequency with the other two events: $\nu = 1.90 \times 10^{13} \text{ s}^{-1}$. If a detrap event occurs, a trapped H atom moves to a 2nd-V-neig-T-site. If the 2nd-V-neig-T-site which is randomly chosen is already occupied, the detrap event is cancelled.

The activation energy for detrap event, $E_{\text{detrapp}}(V_1H_n)$, depends on the number of trapped H atoms, n , as follows:

$$E_{\text{detrapp}}(V_1H_n) = E_{\text{binding}}(V_1H_n) - E_{\text{binding}}(V_1H_{n-1}) + E_{\text{migration}}, \quad (6)$$

where $E_{\text{binding}}(V_1H_n)$ is the binding energy of a complex composed by 1 vacancy and n H atoms, and $E_{\text{migration}}$ is 0.25 eV as described in section 2.1.1. Note that in previous studies [25,26], rate-theoretical models that consider trapping of multiple H atoms by a vacancy and V–H binding energy dependence on the number of trapped H atoms, like the present model, provided good agreement with experimental observation on depth profile and thermal desorption behavior of deuterium irradiated in tungsten.

$E_{\text{binding}}(V_1H_n)$ in Eq. (6) are derived from DFT calculation results reported by Ohsawa et al. [10]. We utilize the data with the zero-point energy correction of atomic vibrations. The resultant $E_{\text{detrapp}}(V_1H_n)$ is shown in Fig. 4 as a function of the number of trapped H atoms, together with $E_{\text{detrapp}}(V_1H_n)$ values determined with results of four other DFT studies [18,27–29]. Two of them [18,27]

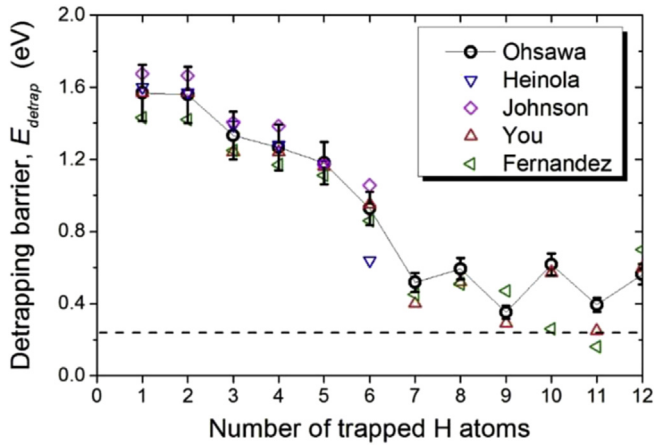


Fig. 4. Energy barriers for detrapp events. The upper and lower bars attached to Ohsawa's data [10] correspond to +10% and –10% variations from the original data. The other data are taken from Ref. [18] (Johnson), Ref. [27] (Heinola), Ref. [28] (You), and [29] (Fernandez).

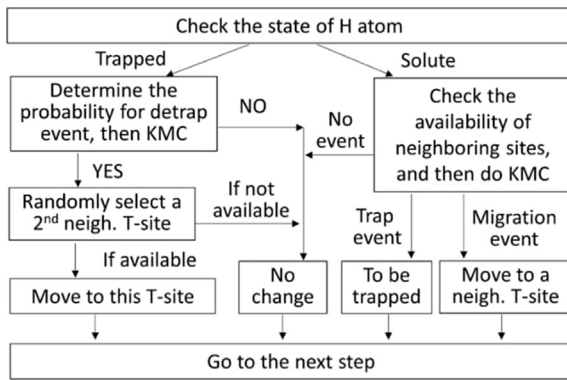


Fig. 5. Computational flow in each KMC simulation step.

Table 1
Kinetic parameters used in the present KMC model.

Event	Attempt frequency, $\nu_{\text{attempt}} \text{ (s}^{-1}\text{)}$	Activation energy, $E \text{ (eV)}$
Migration	1.90×10^{13}	0.25
Trap	1.90×10^{13}	0.25
Detrap	1.90×10^{13}	as in Fig. 4

investigated up to V_1H_6 complex and only considered complexes of high-symmetry configuration. The other two of them [28,29] investigated up to V_1H_{12} complex including complexes of low-symmetry configuration, as the same with Ohsawa's study [10], which give lower energies than high-symmetry configurations and thus more appropriate. As seen in Fig. 4, there are some discrepancies among the five DFT calculation results, although their trends are almost consistent. In order to check the influence of choice of DFT calculation result in KMC simulation results, effects of (1) increase of detrapping energies by 10% and (2) decrease of detrapping energies by 10% from Ohsawa's data are examined. These 10% variations are depicted using upper and lower bars attached to Ohsawa's data in Fig. 4. Most of the available DFT data are encompassed within $\pm 10\%$ range from the data given by Ohsawa.

As a summary, the flow of KMC simulation is described in Fig. 5, and the kinetic parameters of the three events are listed in Table 1.

2.2. KMC simulation conditions

2.2.1. Hydrogen and trap concentrations

Since the main purpose of this study is to verify the Heinola's suggestion on hydrogen diffusivity in tungsten in comparison with Frauenfelder's experiment, KMC simulations need to be done in conditions close to Frauenfelder's experiment. In Frauenfelder's experiment [14], as far as we can read from the paper, a series of degassing experiments were performed after loading hydrogen into a tungsten specimen at the same temperatures with the degassing experiments. The hydrogen loading was made to equilibrate with 600 Torr of H_2 gas. Thus, in the present KMC simulations, the hydrogen concentration is set based on the hydrogen solubility reported in the same Frauenfelder's paper [14]. Specifically, hydrogen concentrations at eight temperatures tested in the present study are as follows in H-atom/W-atom unit: 1.1×10^{-7} (0.11 ppm) at 1023 K, 2.5×10^{-7} (0.25 ppm) at 1103 K, 5.9×10^{-7} (0.59 ppm) at 1197 K, 1.4×10^{-6} (1.4 ppm) at 1307 K, 3.2×10^{-6} (3.2 ppm) at 1441 K, 7.6×10^{-6} (7.6 ppm) at 1605 K, 1.8×10^{-5} (18 ppm) at 1811 K, and 4.2×10^{-5} (42 ppm) at 2078 K.

The concentration of vacancy is determined by referring to an experimental result of Anderl et al. [4], where the trap concentration was estimated to be 2.6×10^{-5} atomic fraction (trap/W-atom) for a sample annealed at 1273 K for 1 h and 1.3×10^{-5} for a sample annealed at 1673 K for 1 h, respectively. The trap energy was estimated to be 1.34–1.42 eV, which is similar to that assumed in the present KMC model. Therefore, we consider that the trap found in Anderl's experiment is a vacancy-type trap or a trap which affects hydrogen diffusivity in a similar manner to a vacancy. In Frauenfelder's experiment, heat treatment was done at 2400 K for more than 10 h (in 600 Torr H_2 gas and in a vacuum) [14]. Thus, the trap concentration should be lower than Anderl's experiment: probably around 1×10^{-5} (10 ppm) or less.

The present KMC model assumes that a vacancy can trap up to twelve H atoms based on the DFT calculation result [10], while Anderl assumed that a trap can capture only one H atom. Considering this difference in the trap capacity, it is reasonable to reduce the vacancy concentration in the present KMC model by a factor of up to 10 from the trap concentration in Anderl's experiment. Consequently, the expected vacancy concentration in Frauenfelder's experiment becomes 1 ppm in the present KMC model. Indeed, the equilibrium concentration of vacancy at the pre-treatment temperature of Frauenfelder's experiment (2400 K) is calculated to be 0.2 ppm using the vacancy formation entropy and enthalpy reported by Rasch et al. [30], which is smaller than but reasonably comparable with the estimate of 1 ppm. Based on the consideration here, we perform KMC simulations with four vacancy concentrations for comparison: 0 ppm (no vacancy), 0.1 ppm, 1 ppm and 10 ppm.

For each simulation condition, to achieve the equilibrium state of the system, more than a few million steps of equilibration run are performed. Then, a diffusion constant is evaluated using the mean square displacement of H atom based on Einstein's relation. Expected errors in determined diffusion coefficients are less than 10%.

2.2.2. Random number generation

In an early stage of KMC simulations, we encountered an unreasonable trend in the time evolution of the means square displacement in some conditions, when a random number generator implemented in a standard C compiler (*rand* function) was utilized. This behavior was due to the unsatisfactory randomness in generated numbers. In addition, a single-precision (24 bit) random number was insufficient to simulate an event of a high activation energy (e.g. 1.568 eV barrier for a detrapp event in V_1H_1 complex). Thus, we utilize a double-precision version (48 bit) of random

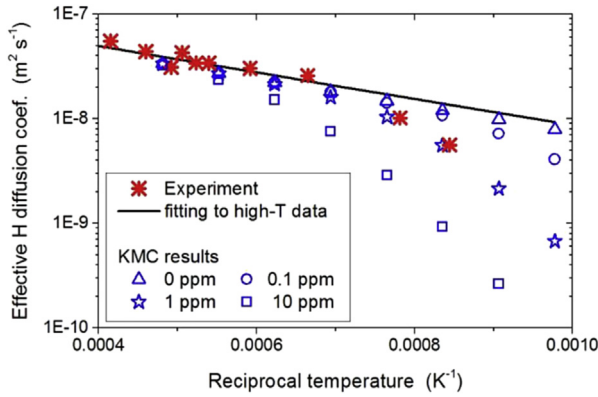


Fig. 6. KMC simulation results on effective hydrogen diffusivities in systems of different vacancy concentrations. The experimental data were taken from Ref. [14]. The fitting line was taken from Ref. [19] as given by Eq. (2) in the present study.

number generator based on an algorithm developed by Lüscher [31], which is implemented in *GNU scientific library* (GSL) as *gsl_rng_ranlxd1*.

3. Results

Fig. 6 compares KMC simulation results with Frauenfelder's experimental data [14] and the formula given by Heinola and Ahlgren [19] (Eq. (2) in the present paper), which was fitted only to high-temperature data (>1500 K) of Frauenfelder's experiment. The KMC results clearly show that the effective hydrogen diffusivity is largely decreased at low temperatures as the vacancy concentration increases. The influence of vacancy is evident below 1600 K when the vacancy concentration is 10 ppm, and below 1300 K when 1 ppm. When the vacancy concentration is 0.1 ppm, the influence is mild even at around 1000 K.

The KMC result of 1 ppm vacancy concentration nicely agrees with all the Frauenfelder's experimental data. As discussed in Section 2.2, 1 ppm is a reasonable value as the expected trap concentration of Frauenfelder's experiment. This agreement underpins the Heinola's interpretation on the gap between theoretical simulation and experimental data [32]: low-temperature data (<1500 K) are largely affected by defects, and then the true coefficients are derived as Eq. (2) by excluding these data. Thus, we recommend $D = 1.58 \times 10^{-7} \exp(-0.25 \text{ eV}/kT) \text{ m}^2 \text{ s}^{-1}$ [32] as the equation for hydrogen diffusion coefficient in bcc-W, rather than the most cited equation $D = 4.1 \times 10^{-7} \exp(-0.39 \text{ eV}/kT) \text{ m}^2 \text{ s}^{-1}$ [14], which is considered to be affected by traps.

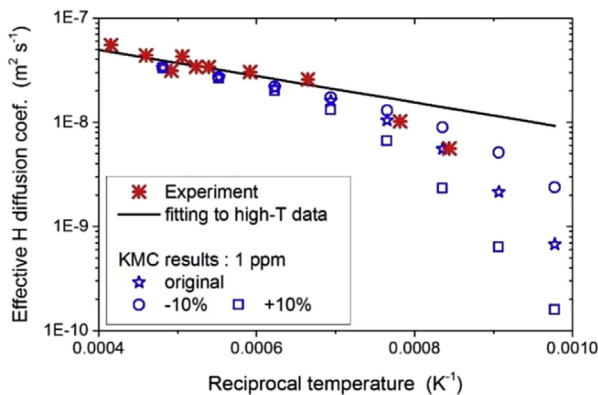


Fig. 7. Effects of detrapping energies variations in KMC simulation results on effective hydrogen diffusivities. The vacancy concentration is fixed at 1 ppm.

Fig. 7 shows influence of $\pm 10\%$ variations of detrapping energies in KMC simulation results. With $+10\%$ variation, we need to assume several times smaller vacancy concentration to achieve nice agreement with Frauenfelder's experiment. With -10% variation, we need to assume several times larger vacancy concentration for nice agreement. For both cases, however, the vacancy concentrations are still within a range of reasonable trap concentrations. Hence, we conclude that the influence of choice of DFT calculation result is not so large to change the results of the present study qualitatively, although the influence is not small.

4. Discussion

In this chapter, we discuss some possible errors in the simple model utilized in the present KMC simulation: influence of vacancy clustering, influence of grain boundary and dislocation, influence of impurity atoms, and influence of quantum effects. None of these influences is not involved in the present KMC simulation.

4.1. Influence of vacancy clustering

In the present model, we do not consider migration of vacancy by relying on the fact that vacancies are far less mobile than hydrogen atoms, as the vacancy migration energy is ~ 1.8 eV [30]. In addition, only isolated mono-vacancies are initially introduced in simulation systems. Thus, vacancy clusters do not appear in the present model.

In experimental studies, formation of vacancy clusters (or voids) is often observed in irradiated tungsten crystals. For example, Eleveld and Veen showed using positron annihilation technique that voids composed by 11–16 vacancies are formed by heating at 650 K after 30 keV D_2^+ ion irradiation at room temperature [33]. Using transmission electron microscopy, Ferroni et al. recently reported a similar observation in tungsten crystals irradiated with 2 MeV W^+ [34]. On the other hands, Frauenfelder's experiment was performed with non-irradiated tungsten crystals, where the vacancy concentration is much lower than that in ion-irradiated tungsten crystals. In addition, the sample pretreatment temperature of Frauenfelder's experiment was 2400 K, which is much higher than the decomposition temperature of voids (1700 K [33]). Hence, we expect that vacancies were not significantly clustered in Frauenfelder's experiment, and then consider that excluding vacancy clusters in KMC simulation is acceptable in the present study. If KMC simulation is performed for ion-irradiated tungsten crystals, modeling of vacancy migration and vacancy clustering should be vital.

The exclusion of vacancy clustering in the present KMC simulation may be also justified from the nature of interactions between H atoms and vacancy clusters. For this, since influence of vacancy clustering on hydrogen diffusivity is yet to be clarified in bcc-W, we refer to knowledge in bcc-Fe. Molecular dynamics simulations in bcc-Fe showed that hydrogen trapping energies in small vacancy clusters are similar to those in a mono-vacancy, if trapping energies are described as a function of H/V ratio [35,36]. For example, the binding energy per H atom is comparable between V_3H_6 complex and V_1H_2 complex. If the binding energies (and thus detrapping energies) are not altered by clustering, trap and detrap models utilized in the KMC simulation do not need to be largely modified.

4.2. Influence of grain boundary and dislocation

Zhou et al. reported a high segregation energy (equivalent with binding energy in the present paper) of 1.11 eV at $\Sigma 5(310)[001]$ tilt grain boundary in tungsten by DFT calculation [21]. Moreover, a vacancy located along the grain boundary heightens the

segregation energy up to around 1.5 eV. The obtained migration energies along this grain boundary is high (e.g. 0.67 eV) [21], and thus the grain boundary purely acts as hydrogen trap like vacancy, although there may be a low-barrier path along another type of grain boundaries. The accumulation of hydrogen on grain boundaries was observed also in experiment [37].

Terentyev et al. showed that dislocation core is a potential trapping site of hydrogen (~ 0.55 eV for $1/2 < 111 >$ screw dislocation) by DFT calculation [22]. This screw dislocation also provides a fast 1-dimensional migration path (0.1 eV as the migration barrier) along the dislocation line. In addition, once eight H atoms are clustered at the dislocation core, they become spontaneously immobile by punching out a jog on the dislocation line. It means that dislocations bring two opposite influences to hydrogen diffusivity, namely decreasing the diffusivity by trapping and increasing the diffusivity by providing a fast path.

Since both grain boundaries and dislocations are inevitably involved in practical materials, it may largely affect tritium retention and release behavior. The effective influence of a trap depends on its strength (trapping energy and capacity), its concentration and the environment (temperature, hydrogen concentration in the system, and the concentration of impurities which occupy some hydrogen trapping sites).

Regarding the trapping capacity, according to DFT calculation, grain boundaries trap two H atoms per vacant structure (the distance between two trapped H atoms is 2.15 Å) [21], while dislocation trap eight or more H atoms per elementary dislocation segment [22]. Regarding the trap concentration, assuming the grain size of a few μm [38], the trap concentration due to grain boundaries is on the order of 100 ppm. If a finer grained material [39] is employed, larger influence of grain boundaries is expected. As for dislocation, dislocation densities of the order of 10^{10} cm^{-2} were reported in tungsten, W–Re and W–Ta alloys [40]. This density approximately corresponds to a trap concentration of the order of 10 ppm in atomic fraction.

Considering the high trap strengths and the estimated trap concentrations, grain boundaries and dislocations should competitively trap hydrogen in practical materials. These defects are formed during manufacturing process, and are additionally formed and evolved by neutron irradiation and by interaction with helium and hydrogen atoms transported from fusion plasma. Therefore, when analyzing experimental results of TDS, the influences of grain boundaries and dislocations should be taken into account in order to reproduce experimental data, even for non-irradiated specimens. Particularly, grain boundaries would affect the hydrogen diffusivity even at high temperatures like Frauenfelder's experiment, due to the large binding energy for hydrogen (1.11 eV [21], corresponding to detrapping energy of ~ 1.3 eV).

4.3. Influence of impurity atoms

In pure W, the concentration of impurities can be suppressed to be less than around 10 weight ppm [41], corresponding to several tens ppm in atomic fraction. Main non-metallic impurities are C and O, as well as He from plasma in fusion reactors. Main metallic impurities are Fe and Mo, as well as Re, Os and Ta as important transmutation products in fusion reactors. The amounts of these transmutation products will reach 0.1% order in the first walls of ITER and % order in the first walls of future power reactors [42].

Regarding the non-metallic impurities, DFT calculation showed that C, O and He can act as weak traps, if these impurity atoms are located at interstitial sites. The hydrogen binding energy is around 0.1 eV for C [43], 0.3 eV for O [43] and 0.2 eV for He [44]. These binding energies are negligibly small compared with binding energies for vacancy.

If a C or O impurity atom is involved as a substitutional impurity for W atom, the situation is largely changed. A study using rate equations with kinetic parameters determined by DFT showed that substitutional C and O atoms have large trapping energies for H atom: 1.25 eV for C and 1.19 eV for O [45], which are comparable with trapping energies by vacancy. Indeed, DFT calculation indicated that substitutional C [46] and O [47] are less stable than interstitial ones by a few eV. However, in a crystal exposed to neutron/ion irradiation, once a substitutional C atom is trapped by a vacancy, the formed complex is stable and quite less mobile [46]. Similar strong interaction between a vacancy and a substitutional O atom is also reported [13]. Then, the complexes may survive for a long time with significantly affecting hydrogen behavior in W. However, as Frauenfelder's experiment is performed with non-irradiated W crystals, it is reasonable to neglect effects of substitutional C and O atoms.

Regarding metallic impurities, DFT calculations showed that hydrogen binding energies for substitutional Re and Os atoms are small (up to ~ 0.3 eV) [27]. Substitutional Ta and Mo atoms have also small hydrogen trapping energies (~ 0.2 eV), while substitutional Fe atom has a relatively large hydrogen binding energy like 0.7 eV [13], although it is still small in comparison with that for a vacancy.

Consequently, as far as we focus on Frauenfelder's experiment at 1100–2400 K, the exclusion of trap effects by the non-metallic and metallic impurities is reasonably justified.

4.4. Influence of quantum effects

In bcc-Fe, an increase of hydrogen diffusivity due to quantum effects such as tunneling effect was clearly observed in path-integral molecular dynamics (PIMD) simulations [48,49]. The crossover temperature between thermal and quantum mechanisms (and thus between classical and quantum regimes) were determined to be 500 K for H [48] and 300 K for T [49]. For tungsten, the crossover temperature was determined by DFT + TST approach with some quantum corrections to be around 200 K for H [19]. However, considering the similarity between bcc-Fe and bcc-W in the solubility and the diffusivity of hydrogen and the larger atomic mass of W than Fe, the true crossover temperature can be higher than 200 K in tungsten. PIMD simulation for hydrogen diffusion in tungsten is necessary to determine the crossover temperature more accurately. Note that the values given by Eq. (2) may underestimate the true hydrogen diffusivity, if quantum effects are significant. However, as far as we focus on the result of Frauenfelder's experiment at 1100–2400 K, it should be reasonable to neglect the quantum effects.

In summary, as far as we study a non-irradiated tungsten crystal at high temperatures (1100–2400 K), focusing on mono-vacancies is a fair simplification. However, as discussed in this chapter, grain boundaries (and probably dislocations) are likely to affect the hydrogen diffusivity in bcc-W even at such high temperatures. Modeling of trap effects of grain boundaries and dislocations in KMC simulation remain as a future work.

Finally, we would like to emphasize one point. Although the present model successfully reproduced Frauenfelder's experimental result with assuming mono-vacancies as traps, it does not mean that mono-vacancy is an only probable trap in Frauenfelder's experiment or other experiments. As discussed in chapter 4, many other traps can affect hydrogen behavior as well. For example, even with grain boundaries, we may reproduce the trend in Frauenfelder's data. Indeed, one weak point of the present study is uncertainty in the vacancy concentration in Frauenfelder's experiment. In Section 2.2.1, we estimated it referring to Anderl's experimental result [4] and to the equilibrium vacancy concentration at the pre-treatment temperature (2400 K). However, the

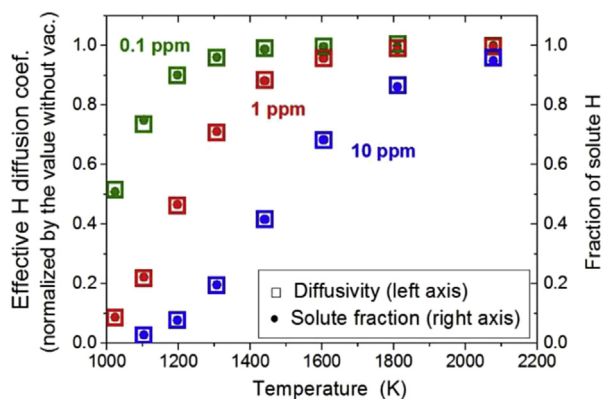


Fig. 8. KMC simulation results on correlation between effective hydrogen diffusivity and fraction of solute hydrogen. The left axis is for the effective diffusivity, while the right axis is for the fraction.

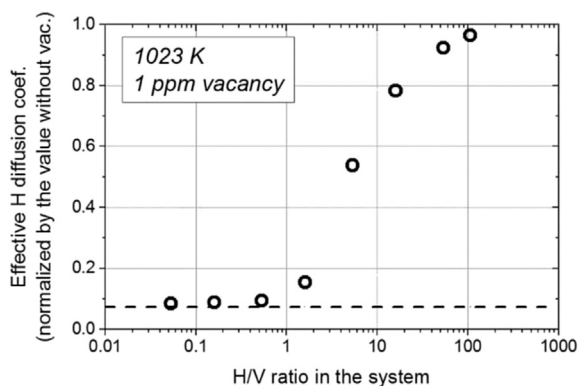


Fig. 9. KMC simulation results on effective hydrogen diffusivities as a function of H/V ratio. The temperatures and the vacancy concentrations are fixed at 1023 K and 1 ppm.

former is not of Frauenfelder's experiment and the trap was not solely attributed to vacancy in Anderl's experiment [4]. The latter does not consider changes of the vacancy concentration during the H₂ gas absorption conducted at lower temperatures than 2400 K. Therefore, at this moment, it would be more appropriate to conclude that trap effects similar to V–H interaction can reproduce Frauenfelder's experimental result, than to conclude that vacancies

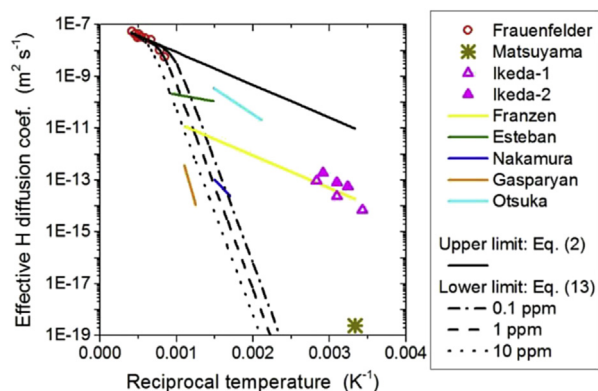


Fig. 10. Comparison between available experimental data and theoretical lower and higher limits of hydrogen diffusivity. The experimental data are taken from Ref. [14] (Frauenfelder), Ref. [52] (Matsuyama), Ref. [53] (Ikeda-1), Ref. [54] (Ikeda-2), Ref. [55] (Franzen), Ref. [56] (Esteban), Ref. [57] (Nakamura), Ref. [51] (Gasparyan), and Ref. [58] (Otsuka).

caused the trend in Frauenfelder's data.

5. Conclusions

KMC simulations were performed to quantify the influence of trap in hydrogen diffusivity in bcc-W. As a typical trap, mono-vacancy is considered. In the KMC simulations, Frauenfelder's experimental results [14] were nicely reproduced when hydrogen and trap concentrations expected in the experiment were assumed in the simulation.

Those KMC results are consistent with the Heinola's interpretation [19] on the data of Frauenfelder's experiment: low-temperature data (<1500 K) are largely affected by defects, and then the true coefficients are better derived if these data are excluded. Therefore, we recommend $D = 1.58 \times 10^{-7} \exp(-0.25 \text{ eV}/kT) \text{ m}^2 \text{ s}^{-1}$ as the equation for hydrogen diffusion coefficient in tungsten, which was derived by Heinola by fitting to high-temperature data of Frauenfelder's experiment [19], rather than the most cited equation $D = 4.1 \times 10^{-7} \exp(-0.39 \text{ eV}/kT) \text{ m}^2 \text{ s}^{-1}$, which was derived by Frauenfelder by fitting to all the experimental data [14]. Since some influences of traps should be mixed up within the original Frauenfelder's equation, its usage may cause a mis-estimation of trap influence. It should be noted that the recommended Heinola's equation also agrees well with DFT + TST calculation results [19], while the original Frauenfelder's equation does not.

Finally, the influences of vacancy clustering, grain boundary and dislocation, impurity atoms, and quantum effects were discussed, none of which were included in the present KMC simulations. Grain boundaries and dislocations are expected to competitively trap hydrogen even at high temperatures, considering their trapping strengths and typical densities. Further studies are needed to construct kinetic models for these traps.

Acknowledgement

This research was supported by National Research Foundation of Korea under Nuclear Fusion Basic Research program. This research was also supported by BK 21 plus project and the Center for Advanced Research in Fusion Reactor Engineering (CARFRE). The calculations in this research were carried out using the HELIOS supercomputer system at the Computational Simulation Center of the International Fusion Research Center (IFERC-CSC) in Japan.

Appendix. Comparison with other experimental results

In Appendix, we further analyze trap effects on the effective hydrogen diffusivity in order to explain why diffusivities reported in previous experiments largely disagree with each other and with Frauenfelder's result.

For this purpose, first we consider the correspondence between the fraction of solute hydrogen atoms and the effective hydrogen diffusivity. When vacancies exist in the lattice, hydrogen diffusion is mostly caused by H atoms solute in the lattice, not H atoms trapped by vacancies. Therefore, the fraction of solute H atoms should be proportional to the effective diffusion coefficient of hydrogen. Fig. 8 compares the fraction and the effective diffusion coefficient in KMC simulation results. The effective diffusion coefficients are normalized by the diffusivity determined in vacancy-free system, which corresponds to 0 ppm data in Fig. 6. A good agreement between the fraction and the normalized effective diffusivity is confirmed. This result means that the effective diffusion coefficient is calculable if the fraction of solute H atoms is known.

Fig. 9 shows a correlation between hydrogen concentration and the normalized effective diffusion coefficient in KMC simulation

results. The temperature and the vacancy concentration are fixed at 1023 K and 1 ppm in the KMC simulation. The hydrogen concentration is given in H/V ratio. For example, the ratio of 1 means that both hydrogen and vacancy concentrations are 1 ppm in reference with the number of lattice sites for W atoms. There are three characteristic regions in Fig. 9: (i) low H/V ratio region ($H/V < 1$), where effective diffusion coefficients are almost constant; (ii) intermediate H/V ratio region ($1 < H/V < 100$), where the effective diffusion coefficient increases as the H/V ratio increases; (iii) high H/V ratio region ($H/V > 100$), where effective diffusion coefficients are comparable with the true diffusion coefficient, which is given by Eq. (2).

Obviously, the upper limit of the effective diffusion coefficient appears in the region (iii) and is equal to the true hydrogen diffusivity. The lower limit can be obtained when the majority of H atoms in a solid is trapped in the most stable state, which are V_1H_1 and V_1H_2 complexes having largest detrapping energy for trapped H atom. This condition is satisfied when the H/V ratio is sufficiently low, because a vacancy hardly traps more than two H atoms in such a system. If more than three H atoms are trapped in a vacancy, the detrapping energy is lowered as seen in Fig. 4. Then, the effective hydrogen diffusivity is escalated as observed in the intermediate H/V ratio region in Fig. 9, because easier detrapping increases the fraction of solute H atoms.

In order to evaluate the lower limit, we consider a system in which one H atom and one vacancy are contained. In this system, interaction between H atoms is totally eliminated and possible V–H interaction is only of V_1H_1 complex, which is consistent with the condition at which the lower limit is achieved. In a steady state of this system, the fraction of trapped H atoms (and the fraction of solute H atoms) are required to be constant. This condition can be formulated by equating the trap rate and the detrap rate, and is described as follows according to the kinetic models for trap and detrap events given in the chapter 2:

$$f_{\text{trap}} \times \Gamma_{\text{detrap}} = 24 \times (f_{\text{solute}}/N_{T\text{-site}}) \times \Gamma_{\text{trap}}, \quad (7)$$

$$f_{\text{trap}} + f_{\text{solute}} = 1, \quad (8)$$

$$\Gamma_{\text{trap}} = \nu_{\text{trap}} \times \exp(-E_{\text{migration}}/kT) \quad (9)$$

$$\Gamma_{\text{detrap}} = \nu_{\text{detrap}} \times \exp(-E_{\text{detrap}}/kT), \quad (10)$$

$$c_{\text{vacancy}} = N_{\text{vacancy}}/N_{\text{lattice-site}} = 1/N_{\text{lattice-site}}, \quad (11)$$

$$N_{T\text{-site}} = 6N_{\text{lattice-site}}. \quad (12)$$

Eq. (7) represents the balance between the flux of H atoms from a solute state to a trapped state and the flux of the opposite direction. The former flux corresponds to the jump rate of H atoms from 2nd-V-neig-T-sites to 1st-V-neig-T-sites, and the latter to that from 1st-V-neig-T-sites to 2nd-V-neig-T-sites. f_{trap} and f_{solute} correspond to the fractions of trapped H atoms and solute H atoms, respectively, and they need to satisfy Eq. (8). The factor 24 in Eq. (7) reflects the number of 2nd-V-neig-T-sites, from which solute H atoms may jump into 1st-V-neig-T-sites in the trap process. Eqs. (9) and (10) give the rates of trap and detrap events per H atom, Γ_{trap} (s^{-1}) and Γ_{detrap} (s^{-1}), respectively, where $E_{\text{migration}} = 0.25$ eV and $E_{\text{detrap}} = 1.568$ eV are set, as V_1H_1 is only a possible trap state in this system. Eqs. (11) and (12) show the correlation among the vacancy concentration (c_{vacancy} , in atomic fraction), the number of vacancies (N_{vacancy} ; equal to 1 here), the number of T-sites ($N_{T\text{-site}}$), and the number of lattice sites where W atoms originally occupy ($N_{\text{lattice-}}$

site). The factor 6 in Eq. (12) reflects the fact that the number of T-sites in bcc-lattice is 6 times as many as the number of lattice sites of constituent atoms. Finally, Eqs. 7–12 are combined into

$$f_{\text{solute}} = \Gamma_{\text{detrap}} / (\Gamma_{\text{detrap}} + 4c_{\text{vacancy}}\Gamma_{\text{trap}}) \\ = 1 / (1 + 4c_{\text{vacancy}} \times \exp(E_{\text{binding}}/kT)). \quad (13)$$

Note that this resultant equation is almost identical to the classic McNabb and Forster formula [50] for the effective diffusion coefficient in the field of defects [51], except for the factor 4.

As a validation test of Eq. (13), f_{solute} is determined in the condition of the KMC simulation of Fig. 9, where $c_{\text{vacancy}} = 1 \times 10^{-6}$ (1 ppm) and $T = 1023$ K are set. Then, f_{solute} is calculated to be 0.0736, which is indicated by a broken line in Fig. 9. Since f_{solute} is equal to the normalized effective diffusivity of hydrogen, the broken line correctly delineates the lower limit of effective diffusion coefficient in Fig. 9. Strictly speaking, the effective hydrogen diffusivity still depends on H/V ration in the low H/V ratio region. This is because even for $H/V < 1$ region, V_1H_2 , V_1H_3 and other complexes can be formed with certain probabilities in reality and in the KMC simulation. Therefore, although the H/V dependence in the low H/V ratio region is much weaker than the intermediate H/V ratio region, a decrease of H/V ratio still slightly lowers the effective hydrogen diffusivity.

Fig. 10 compares (i) the upper limit of the effective hydrogen diffusivity, which is given by Eq. (2) as the true hydrogen diffusivity in the bulk, (ii) the lower limit of the effective hydrogen diffusivity in systems where vacancies act as trap, which is given by Eq. (13), and (iii) available experimental results [51–58] other than the Frauenfelder's result [14]. Almost all the experimental data are encompassed by the upper and lower limits, although the spanned range is quite broad due to the large detrap energy for H atom in V_1H_1 complex (1.568 eV). Strictly speaking, the data given by Gasparyan et al. is smaller than the lower limit. However, this deviation is acceptably small considering possible errors and uncertainties in the present model: (i) Eq. (2) should contain some errors from the true hydrogen diffusivity, because it was derived from experimental data of a sole study [19]; (ii) V–H binding energies given by DFT should contain some errors; (iii) only vacancy is taken into account as a hydrogen trap in the present KMC simulation and simple trap/detrap models are utilized; (iv) the experimental data of Gasparyan is also not free of errors.

In experiments, the effective diffusivity of hydrogen is usually defined as a function of temperature, although it also depends on hydrogen concentration, trap concentration and trap type. The dependencies on hydrogen concentration and trap concentration basically become negligible at high temperatures. However, for a deep trap like vacancies, these dependencies cannot be neglected up to around 1500 K in bcc-W, as demonstrated in the present study. Therefore, it is reasonable to assume that H/V ratios in most previous experiments are of the intermediate H/V ratio region or of the low H/V ratio region given in Fig. 9. In the intermediate H/V ratio region, effective hydrogen diffusivities are very sensitive to experimental conditions, which would cause inconsistent results on effective hydrogen diffusivities in previous experiments.

References

- [1] M.A. Abdou, E.L. Vold, C.Y. Gung, M.Z. Youssef, K. Shin, *Fusion Technol.* 9 (1986) 250.
- [2] M. Nishikawa, T. Tanabe, *Fusion Eng. Des.* 85 (2010) 987.
- [3] K. Heinola, T. Ahlgren, *Phys. Rev. B* 81 (2010) 073409.
- [4] R.A. Anderl, D.F. Holland, G.R. Longhurst, R.J. Pawelko, C.L. Trybus, C.H. Sellers, *Fusion Technol.* 21 (1992) 745.
- [5] J. Roth, E. Tsitrone, T. Loarer, V. Philipps, S. Brezinsek, A. Loarte, G.F. Counsell, R.P. Doerner, K. Schmid, O.V. Ogorodnikova, R.A. Causey, *Plasma Phys. Control.*

- Fusion 50 (2008) 103001.
- [6] M. Fukumoto, H. Kashiwagi, Y. Ohtsuka, Y. Ueda, M. Taniguchi, T. Inoue, K. Sakamoto, J. Yagyu, T. Arai, I. Takagi, T. Kawamura, J. Nucl. Mater 390–391 (2009) 572.
- [7] M. Shimada, Y. Hatano, P. Calderoni, T. Oda, Y. Oya, M. Sokolov, K. Zhang, G. Cao, R. Kolasinski, J.P. Sharpe, J. Nucl. Mater 415 (2011) S667.
- [8] Y. Hatano, M. Shimada, T. Otsuka, Y. Oya, V.K. Alimov, M. Hara, J. Shi, M. Kobayashi, T. Oda, G. Cao, K. Okuno, T. Tanaka, K. Sugiyama, J. Roth, B. Tyburska-Püschel, J. Dörner, N. Yoshida, N. Futagami, H. Watanabe, M. Hatakeyama, H. Kurishita, M. Sokolov, Y. Katoh, Nucl. Fusion 53 (2013) 073006.
- [9] Y.L. Liu, Y. Zhang, H.B. Zhou, G.H. Lu, F. Liu, G.N. Luo, Phys. Rev. B 79 (2009) 1.
- [10] K. Ohsawa, J. Goto, M. Yamakami, M. Yamaguchi, M. Yagi, Phys. Rev. B 82 (2010) 184117.
- [11] T. Tanabe, Phys. Scr. T159 (2014) 014044.
- [12] K. Nordlund, C. Björkas, T. Ahlgren, A. Lasa, a E. Sand, J. Phys. D. 47 (2014) 224018.
- [13] G.H. Lu, H.B. Zhou, C.S. Becquart, Nucl. Fusion 54 (2014) 086001.
- [14] R. Frauenfelder, J. Vac. Sci. Technol. 6 (1969) 388.
- [15] D. Jiang, E. Carter, Phys. Rev. B 70 (2004) 064102.
- [16] D.C. Sorescu, Catal. Today 105 (2005) 44.
- [17] Y.L. Liu, Y. Zhang, G.N. Luo, G.H. Lu, J. Nucl. Mater 390–391 (2009) 1032.
- [18] D.F. Johnson, E.A. Carter, J. Mater. Res. 25 (2011) 315.
- [19] K. Heinola, T. Ahlgren, J. Appl. Phys. 107 (2010) 113531.
- [20] E. Serra, G. Benamati, O.V. Ogorodnikova, J. Nucl. Mater 255 (1998) 105.
- [21] H.B. Zhou, Y.L. Liu, S. Jin, Y. Zhang, G.N. Luo, G.H. Lu, Nucl. Fusion 50 (2010) 025016.
- [22] D. Terentyev, V. Dubinko, A. Bakaev, Y. Zayachuk, W. Van Renterghem, P. Grigorev, Nucl. Fusion 54 (2014) 042004.
- [23] G.K. White, M.L. Mingos, Int. J. Thermophys. 18 (1997) 1269.
- [24] L.S. Dubrovinsky, S.K. Saxena, Phys. Chem. Min. 24 (1997) 547.
- [25] T. Ahlgren, K. Heinola, K. Vörtler, J. Keinonen, J. Nucl. Mater 427 (2012) 152.
- [26] K. Schmid, U. von Toussaint, T. Schwarz-Selinger, J. Appl. Phys. 116 (2014) 134901.
- [27] K. Heinola, T. Ahlgren, K. Nordlund, J. Keinonen, Phys. Rev. B 82 (2010) 094102.
- [28] Y.W. You, X.S. Kong, X.B. Wu, Y.C. Xu, Q.F. Fang, J.L. Chen, G.N. Luo, C.S. Liu, B.C. Pan, Z. Wang, AIP Adv. 3 (2013) 012118.
- [29] N. Fernandez, Y. Ferro, D. Kato, Acta Mater 94 (2015) 307.
- [30] K.D. Rasch, R.W. Siegel, H. Schultz, Philos. Mag. A 41 (1980) 91.
- [31] M. Luescher, Comput. Phys. Commun. 79 (1994) 100.
- [32] T. Ahlgren, K. Heinola, N. Juslin, A. Kuronen, J. Appl. Phys. 107 (2010) 033516.
- [33] H. Eleveid, A. van Veen, J. Nucl. Mater 212–215 (1994) 1421.
- [34] F. Ferroni, X. Yi, K. Arakawa, S.P. Fitzgerald, P.D. Edmondson, S.G. Roberts, Acta Mater 90 (2015) 380.
- [35] E. Hayward, C. Deo, J. Phys. Condens. Matter 23 (2011) 425402.
- [36] J. Maisonneuve, T. Oda, S. Tanaka, Fusion Sci. Technol. 60 (2011) 1507.
- [37] K. Isobe, V. Alimov, A. Taguchi, J. Plasma Fusion Res. 10 (2013) 81.
- [38] V.K. Alimov, B. Tyburska-Püschel, S. Lindig, Y. Hatano, M. Balden, J. Roth, K. Isobe, M. Matsuyama, T. Yamanishi, J. Nucl. Mater 420 (2012) 519.
- [39] H. Kurishita, H. Arakawa, S. Matsuo, T. Sakamoto, S. Kobayashi, K. Nakai, G. Pintsuk, J. Linke, S. Tsurekawa, V. Yardley, K. Tokunaga, T. Takida, M. Katoh, A. Ikegaya, Y. Ueda, M. Kawai, N. Yoshida, Mater. Trans. 54 (2013) 456.
- [40] J.R. Stephens, Metall. Mater. Trans. 1 (1970) 1293.
- [41] PLANSEE, <http://www.plansee.com/en/893.htm>.
- [42] M.R. Gilbert, J.C. Sublet, Nucl. Fusion 51 (2011) 043005.
- [43] X.S. Kong, Y.W. You, Q.F. Fang, C.S. Liu, J.L. Chen, G.N. Luo, B.C. Pan, Z. Wang, J. Nucl. Mater 433 (2013) 357.
- [44] C.S. Becquart, C. Domain, J. Nucl. Mater 386–388 (2009) 109.
- [45] K. Heinola, T. Ahlgren, J. Nucl. Mater 438 (2013) S1001.
- [46] Y.L. Liu, H.B. Zhou, S. Jin, Y. Zhang, G.H. Lu, J. Phys. Condens. Matter 22 (2010) 445504.
- [47] A. Alkhamees, Y.L. Liu, H.B. Zhou, S. Jin, Y. Zhang, G.H. Lu, J. Nucl. Mater 393 (2009) 508.
- [48] H. Kimizuka, H. Mori, S. Ogata, Phys. Rev. B 83 (2011) 094110.
- [49] T. Yoshikawa, T. Takayanagi, H. Kimizuka, M. Shiga, J. Phys. Chem. C 116 (2012) 23113.
- [50] A. McNabb, P.K. Foster, Trans. Metall. Soc. AIME 227 (1963) 618.
- [51] Y.M. Gasparyan, A.V. Golubeva, M. Mayer, A.A. Pisarev, J. Roth, J. Nucl. Mater 390–391 (2009) 606.
- [52] M. Matsuyama, T. Murai, K. Yoshida, K. Watanabe, H. Iwakiri, N. Yoshida, J. Nucl. Mater 307–311 (2002) 729.
- [53] T. Ikeda, T. Otsuka, T. Tanabe, J. Nucl. Mater 415 (2011) S684.
- [54] T. Ikeda, T. Otsuka, T. Tanabe, Fusion Sci. Technol. 60 (2011) 1463.
- [55] P. Franzen, C. Garcia-Rosales, H. Plank, V.K. Alimov, J. Nucl. Mater 241–243 (1997) 1082.
- [56] G.A. Esteban, A. Perujo, L.A. Sedano, K. Douglas, J. Nucl. Mater 295 (2001) 49.
- [57] H. Nakamura, W. Shu, T. Hayashi, M. Nishi, J. Nucl. Mater 313–316 (2003) 679.
- [58] T. Otsuka, T. Hoshihira, T. Tanabe, Phys. Scr. T138 (2009) 014052.